DNA methylation either antagonizes or promotes Polycomb recruitment at transposable elements

Valentin Hure[1], Florence Piron-Prunier[1] and Angélique Déléris[1]

[1] Université Paris-Saclay, Commissariat à l'Energie Atomique (CEA), Centre National de la Recherche Scientifique (CNRS), Institute for Integrative Biology of the Cell (I2BC), 91190, Gif-sur-Yvette, France

ABSTRACT

Transposable elements (TEs) are primarily silenced by DNA methylation and the associated histone modification H3K9me2 in many multicellular eukaryotes, including plants. However, in the absence of DNA methylation due to mutations in the DNA methylation machinery or in certain developmental contexts, the same TEs can gain Polycomb-associated H3K27me3, another epigenetic silencing mark that is usually linked with the facultative silencing of genes. In this study, we initially aimed to investigate whether DNA methylation and H3K27me3 could compete during the establishment of silencing at TEs in the model plant Arabidopsis. Strikingly, we show that the deposition of the H3K27me3 mark at newly inserted transgenic TE sequences is impaired in plants in which the *de novo* DNA methyltransferase DRM2 is mutated, contrary to the competition model hypothesized. Further profiling of H3K27me3 in *drm2* mutants and in the DNA demethylase mutant *rdd* confirmed this new role of DNA methylation in promoting H3K27me3 deposition at some loci, in addition to the previously described antagonistic role at others; these findings further reveal a new function of DNA demethylation in modulating H3K27me3 levels in vegetative tissues. Finally, by implementing targeted DNA methylation

experiments, we demonstrate that DNA methylation has a direct impact on PcG recruitment and can either promote H3K27me3 deposition or antagonize it in a locus-specific manner. Together, our results uncover a novel crosstalk between DNA methylation and Polycomb and reveal that these two pathways, thought to be specialized and antagonistic, can be interdependent and cooperate more than anticipated to maintain genome and epigenome integrity in eukaryotes.

INTRODUCTION

Transposable elements (TEs) are repetitive DNA sequences that have the potential to multiply and move around the genome, thus compromising genome integrity[1]. Nevertheless, this threat is largely mitigated by genome defense mechanisms that efficiently target transposable elements and stably repress their expression across cell division and generations through epigenetic marks such as DNA methylation (5mC). These marks can persist even on TEs that have aged and lost mobility and such DNA-methylated TEs can play a role as epigenetic regulatory modules that can impact nearby gene regulation[1]. In plants and *Arabidopsis thaliana*, DNA methylation is established and maintained by three classes of DNA methyltransferases. METHYLTRANSFERASE 1 (MET1) maintains CG methylation while CHROMOMETHYLASE 3 (CMT3) and CHROMOMETHYLASE 2 (CMT2) maintain CHG and CHH methylation respectively, and ensure feedback loops with H3K9me2 histone methyltransferases[2]. DOMAINS REARRANGED METHYLASE 2 also maintains non-CG methylation, CHH mainly _at TE loci that are smaller than those targeted by CMT2_ and CHG to a lesser extent _in cooperation with CMT3_[3], and possibly contributes to CG methylation[2,4]. Importantly, DRM2 is able to methylate DNA *de novo* in all sequence contexts as part of the RNA-directed DNA methylation (RdDM) pathway guided by small RNAs (also referred to as

51 small-interfering RNAs or siRNAs)[3]. Thus, *drm2* mutation drastically impairs *de novo*
52 methylation of newly inserted repeats or TE-derived sequences[5,6], a molecular phenotype also
53 observed to various extents in mutants for RNA interference or RdDM factors connected to
54 DRM2 activity[6,7].

55 The detection of a TE that precedes its *de novo* methylation can be achieved in two
56 manners[8]. The first, referred to as "expression-dependent silencing", is based on TE transcript
57 detection by the RNA interference machinery, which leads to the production of small RNAs[7].
58 These small RNAs can mediate not only transcript degradation but also RNA-directed DNA
59 methylation by guiding DRM2 to homologous sequences[3]. Alternatively, if the TE is not
60 transcribed upon insertion but displays sequence homology with another DNA-methylated TE
61 copy that accumulates small RNAs in the genome, then the preexisting small RNAs can
62 similarly guide the *de novo* deposition of DNA methylation by DRM2 by virtue of sequence
63 homology with the TE neo-copies ("homology-dependent silencing")[8]. The initial DNA
64 methylation levels on a newly introduced repeat-containing transgene or a TE neo-insertion are
65 usually not as high as those of the corresponding endogenous copy, and several generations are
66 needed to reach these levels and a stably repressed state[9,10].

67 While very stable across generations and over evolutionary time, the DNA methylation
68 patterns can nonetheless be constitutively pruned by the four members of the DEMETER
69 (DME) family of 5-methylcytosine DNA glycosylases named DME (DEMETER), ROS1
70 (REPRESSOR OF SILENCING 1), DML2 and DML3 (DEMETER-LIKE 2 and 3). These
71 DNA demethylases act both redundantly and in a locus-specific manner in vegetative tissues to
72 counteract excessive DNA methylation[11–14]. DME (DEMETER), in particular, demethylates
73 transposable elements in companion cells of male and female gametophytes[15,16] and is required
74 to establish imprints in the endosperm[17]. In contrast to DNA methyltransferases, which have
75 sequence context-dependent activities, DNA glycosylases can demethylate 5mC regardless of

76 the sequence context[12,18,19]. Several functions have been shown for active DNA demethylation,
77 such as preventing the spread of DNA methylation outside of primary targeted sequences[11] or
78 actively participating in gene control, either at specific stages of development[20] or by preventing
79 stress-responsive genes from being locked in a constitutively silent state[21,22].

80 Interestingly, in recent years, TEs have been shown to be decorated by another
81 epigenetic silencing mark, H3K27me3 (trimethylation of lysine 27 of Histone 3)[23] associated
82 with the evolutionary conserved Polycomb-group (PcG) proteins. This pathway mediates a
83 more dynamic form of transcriptional repression than DNA methylation and has long been
84 thought to specifically target protein-coding genes, particularly development genes for
85 establishing cell identity, or stress-responsive genes[24,25]. H3K27me3 is catalyzed by Polycomb
86 Repressive Complex 2 (PRC2), which is composed of four subunits and is present as different
87 PRC2 cores in Arabidopsis. The catalytic activity is performed by either CURLY LEAF (CLF),
88 SWINGER (SWN) or MEDEA (MEA), which are the three plant homologs of animal
89 ENHANCER OF ZESTE HOMOLOG 2 (EZH2)[23,25]. PRC2 is associated with PRC1, which is
90 composed of two core subunits and mediates the ubiquitination of H2A (H2Aub) to allow a
91 silent yet responsive transcriptional state of H3K27me3-marked targets[23]. In Arabidopsis, the
92 recruitment of PRC2 to genes has been shown to be mediated via Transcription Factors (TF)
93 that can recognize short recognition sequence motifs called Polycomb responsive elements
94 (PREs), and that were initially described for the recruitment of PRC2 to Drosophila genes[23].
95 Long noncoding RNAs have also been involved in PRC2 targeting to genes[26,27]. Finally, PRC2
96 recruitment was shown at some loci to be dependent on the presence of PRC1 and H2Aub[23].

97 Interestingly, in recent years, PcG has appeared to be the dominant system for silencing
98 TEs in wild-type unicellular eukaryotes and plants from early lineages, thus illustrating the
99 ancient role of PcG in regulating TE silencing[23,28]. However, in Arabidopsis, PcG can be
100 recruited to three types of TEs[29]. First, approximately one-third of DNA-methylated TEs can

101 gain H3K27me3 in mutants impaired for DNA methylation, such as *met1* or *ddm1*[30–32,] or in
102 specific cell types that are naturally hypomethylated[33]. This finding implies that DNA
103 methylation, particularly CG methylation, can exclude H3K27me3 deposition. Nevertheless, in
104 some instances, the two marks can co-localize at the molecule level[34–36,] and this was proposed
105 to be constrained by DNA methylation density[34,36]. In this context, the two marks can cooperate
106 in restricting TE activation, for example upon biotic stress[36]. Finally, we recently reported that
107 many TE are targeted by the H3K27me3 histone mark in the genome of wild type Arabidopsis
108 plants "instead of" DNA methylation, not only short TE relics but also relatively intact copies[29].
109 Whether active DNA demethylation can promote H3K27me3 recruitment in some of these
110 cases is unknown.
111
112 In this study, we aimed to further investigate the crosstalk between DNA methylation
113 and PcG proteins and reveal novel relationships between these pathways at TEs. Using neo-
114 inserted TE transgenic sequences that are able to recruit both H3K27me3 and DNA methylation
115 *de novo,* we provide evidence that the deposition of H3K27me3 is dependent on DRM2. This
116 finding sheds light on an unsuspected interconnection between the PcG and RdDM pathways
117 and points to a positive crosstalk between them in that context of TE neo-insertion, rather than
118 the antagonism previously proposed. We further identified a subset of endogenous loci that lose
119 H3K27me3 upon the loss of non-CG methylation maintenance in *drm2*, in addition to an
120 anticipated subset where the loss of non-CG methylation leads to an increase in H3K27me3.
121 These results highlight a dual, locus-specific effect of DNA methylation on PcG recruitment.
122 Accordingly, in the *ros1 dml2 dml3* triple mutant, the gain of 5mC leads to the gain of
123 H3K27me3 at some loci but also to the loss of H3K27me3 at others, and this effect was
124 validated by targeted DNA methylation experiments. Hence, these findings also reveal a novel
125 function of DNA demethylases in the modulation of H3K27me3 via DNA demethylation.

126 Together, our results uncover new interdependencies between DNA methylation and the
127 Polycomb machinery, particularly in the context of TE neo-insertion. Thus, the two major
128 silencing pathways, generally thought to separated, cooperate to shape the epigenome, a
129 concept that could extend to other multicellular eukaryotes.
130

131 # RESULTS

132 **DRM2 is involved in the establishment of H3K27me3 at a newly inserted TE sequence.**

133 We previously showed that neo-inserted, transgenic sequences of the mobile
134 *ATCOPIA21* retrotransposon (*AT5TE65370*) consistently recruit H3K27me3 *de novo*[29]. The
135 endogenous copy is DNA methylated in WT plants and accumulates 24-nt siRNAs (**Fig. S1A**)
136 that are likely to target RNA-directed *de novo* DNA methylation to the homologous transgenic
137 sequences. To verify this, we performed BS-seq on the pools of primary *COPIA21*
138 transformants (TR) used for H3K27me3 analysis [29]. We determined that the transgenic copies
139 are indeed DNA methylated and that they are less DNA methylated than the endogenous copies
140 except in the CHH context (**Fig. 1A**). This higher CHH methylation at transgenes is caused by
141 high *de novo* CHH methylation of the long-terminal repeats (LTR) (**Fig. 1A**), presumably
142 because small RNAs corresponding to these sequences are particularly abundant in WT plants
143 (**Fig. S1A**).As expected, the DNA methylation levels at other TEs in the genome are unchanged
144 upon *ATCOPIA21* sequence insertion (**Fig. S1B**).

145 To test a model of competition between DNA methylation and H3K27me3 in this
146 context of neo-insertion, we transformed the *ATCOPIA21* construct into WT and *drm2* mutant
147 plants impaired in *de novo* DNA methylation. We assessed H3K27me3 levels at the neo-
148 inserted sequences in large pools of primary transformants of the same size for each genetic
149 background. Surprisingly, we observed a drastic and reproducible decrease in H3K27me3 at
150 *ATCOPIA21* copies in the *drm2* mutant plants compared with the WT plants (**Fig. 1B**). This

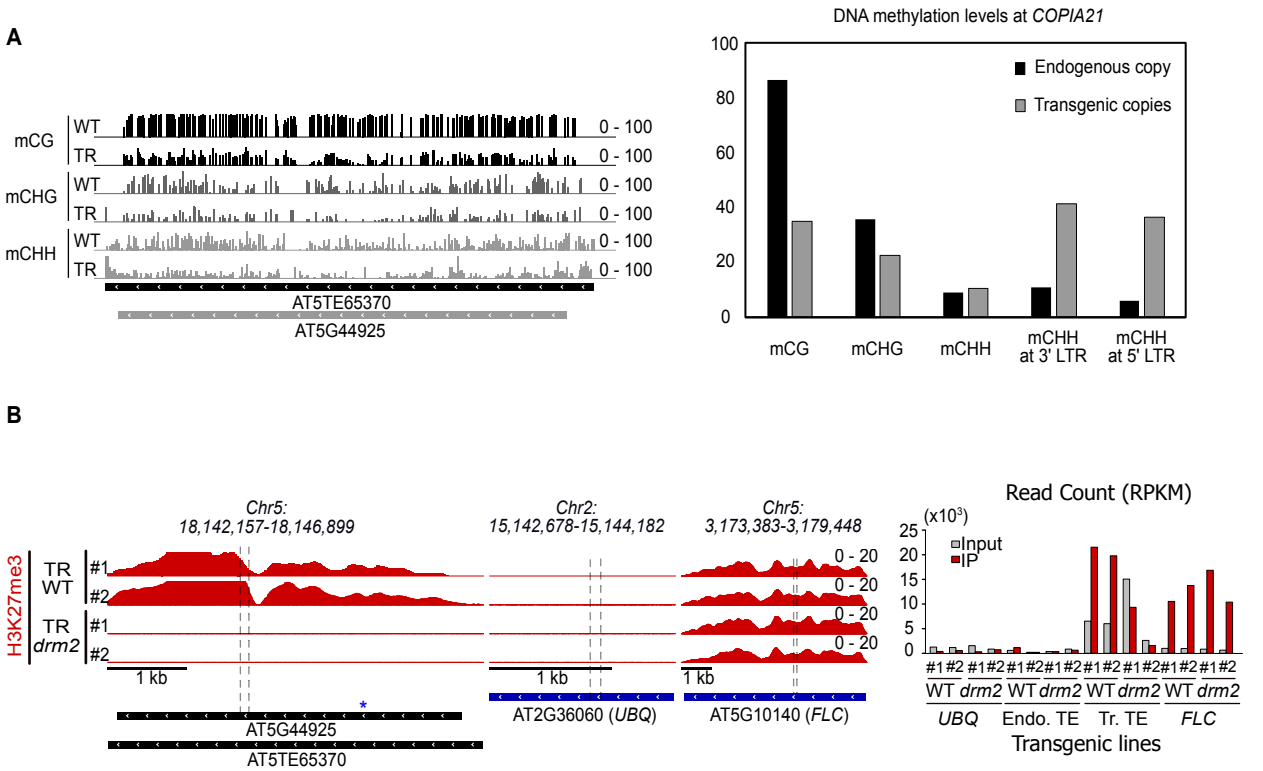

Figure 1. Role of DRM2 in the establishment of *de novo* H3K27me3 at a neo-inserted TE transgenic sequence. **(A) Left panel**: Representative genome browser view of DNA methylation status (CG : black, CHG : dark grey, CHH : light grey) at *COPIA21* in untransformed wild-type (WT) platns and in pools of primary transformants with transgenic *COPIA21* sequence (TR). **Right panel**: Barplot showing the DNA methylation levels in each context at *COPIA21* (AT5TE65370) endogenous copy (black bars) and transgenic copies (grey bars). **(B) Left panel.** Representative genome browser view of H3K27me3 average profile (IP over INPUT) at *COPIA21* sequence in two independent pools of plants transformed with *COPIA21* transgene (#1 and #2) either in WT (Col-0)(upper lanes) or in *drm2* mutant (lower lanes). The H3K27me3 signal in these tracks reflects the H3K27me3 status at the endogene + transgene (SNP as blue star). **Middle panel**: *UBQ* and *FLC* are shown as negative and positive controls respectively for H3K27me3 recruitment. **Right panel:** Recruitment on the transgene is assessed by quantification of endogenous and transgenic *COPIA21* sequences immuno-precipitated with H3K27me3 using ChIP-seq reads at the region where a SNP was introduced to discriminate transgene and endogene: reads overlapping with the SNP at *COPIA21* locus were extracted, counted and normalized by the total read number. Recruitment on the transgene is validated by the enrichment observed in the IP as compared to an the Input fraction. At control regions (*UBQ* and *FLC*), reads were extracted at positions *Chr5:3,178,750* (1st intron) and *Chr2:15,143,214,* respectively. Copy number variation between transgenic pools can be visualized with the Input DNA fraction (grey bar).

151 finding reveals that DRM2 is required for the *de novo* deposition of H3K27me3 at newly TE
152 inserted sequences.
153
154 **DRM2 is involved in the maintenance of H3K27me3 at endogenous TEs.**
155 Next, we profiled H3K27me3 in *drm2* mutants and observed globally unchanged
156 H3K27me3 levels at genes and endogenous TEs (**Fig. S2A**). Thus, DRM2 is neither necessary
157 for general PRC2 activity nor has indirect effects on the PcG machinery.
158 Closer data inspection and stringent analysis revealed an increase in H3K27me3 in *drm2*
159 plants at a small subset of loci (*i.e.* H3K27me3 peak gain in *drm2*, **Fig. 2A** and **Fig.2B, S2B**).
160 Loss of non-CG methylation at these loci further confirms that they are DRM2 targets (**Fig.**
161 **S2C**). This indicates that DRM2-dependent DNA methylation can antagonize H3K27me3
162 deposition, as previously described for CG methylation[31,32]. Of note, the extent of H3K27me3
163 gain did not seem proportional to the extent of CHH loss, possibly because the loss of discrete
164 critical cytosines could be sufficient to allow H3K27me3 deposition (**Fig.S2B**, yellow regions
165 and arrows).
166 On the other hand,, we observed a drastic loss of H3K27me3 in *drm2* at another subset
167 of loci (*i.e.* H3K27me3-peak complete loss in *drm2*, **Fig. 2C and Fig.2D, S2D**), which is in
168 line with the observations at the *ATCOPIA21* transgene. Again, loss of non-CG DNA
169 methylation at these loci further confirms that they are DRM2 targets (**Fig. S2E).** Like for the
170 other subset, the extent of H3K27me3 loss did not seem proportional to the extent of CHH loss,
171 possibly because the loss of several given cytosines may be sufficient to induce a decrease in
172 H3K27me3 levels (**Fig. S2D**, yellow regions and arrows). These results indicate that DRM2-
173 mediated maintenance of CHH methylation at a subset of loci can be important for proper
174 H3K27me3 patterning, although a DNA methylation-independent role of DRM2 cannot be
175 excluded.

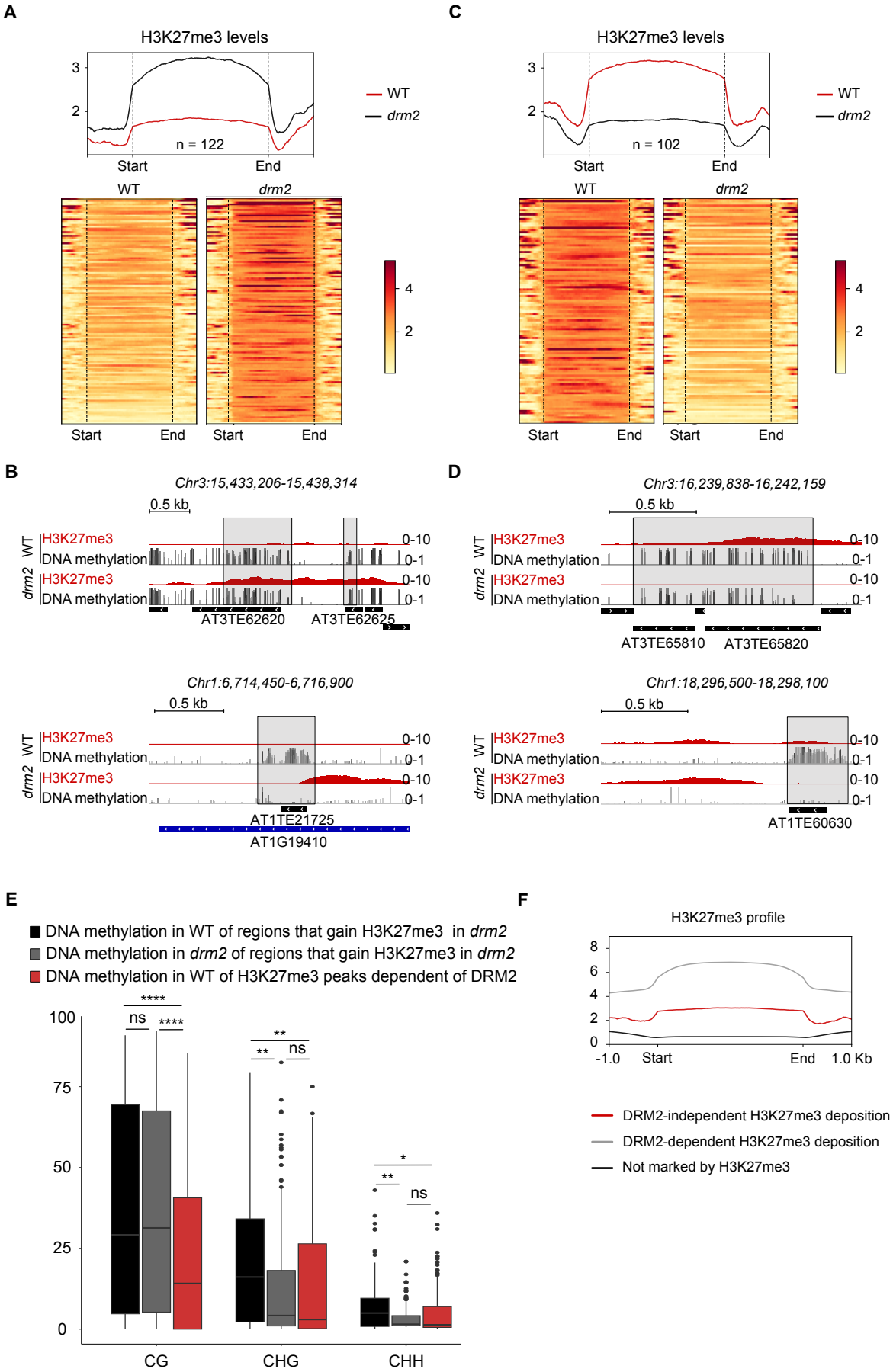

Figure 2. Role of DRM2 in the recruitment of H3K27me3 at endogenous loci.
(A) Heatmaps and metagenes showing H3K27me3 levels for loci that gain H3K27me3 peaks in *drm2* compared to WT. **(B)** Representative genome browser views showing H3K27me3 ChIP-seq and DNA methylation BS-seq data in WT and *drm2* mutant. Published differentially methylated regions (DMRs) are shown with grey boxes (*Stroud et al, 2013*). **(C)** Heatmaps and metagenes showing H3K27me3 levels for loci that loose H3K27me3 peaks in *drm2* compared to WT. **(D)** Representative genome browser views showing H3K27me3 and DNA methylation data in WT and *drm2* mutant. Loss of H3K27me3 in *drm2* compared to WT is associated with previously published DMRs (grey boxes) (*Stroud et al, 2013*). **(E)** Boxplot showing DNA methylation in three contexts for different H3K27me3 peaks regions (i.e. peak+500bp on the sides to account for any effect of DNA methylation patches on peak edges). Black and grey bars show the DNA methylation levels in the same regions, either in WT or in *drm2*, respectively. These regions correspond to peaks of H3K27me3 gained in *drm2* mutant. Red bars show DNA methylation levels at peaks where H3K27me3 is dependent on DRM2. Statistical analyses were performed using Wilcoxon-Mann-Whitney U-test. ns = not significant; * = p-value < 0.05; ** = p-value < 0.01; *** = p-value < 0.001. **(F)** Metaplots showing H3K27me3 profiles at loci marked by H3K27me3 dependently (grey) or independently of DRM2 (red); non-H3K27me3 loci are shown as negative control (black).

176 We next aimed to further characterize the contexts in which H3K27me3 deposition is
177 dependent on DRM2 (i.e 1,2% of the H3K27me3 peaks). Loci where H3K27me3 marks are
178 promoted by DRM2 and co-localize with DNA methylation (**Fig. 2E**, red bars) are significantly
179 less DNA methylated, in all three sequence contexts than loci where H3K27me3 marks are
180 antagonized by DRM2 (**Fig.2E**, black bars). This suggests that a certain threshold of DNA
181 methylation may contribute to determine whether H327me3 deposition is antagonized (high
182 DNA methylation) or promoted (low DNA methylation) by DRM2. In support of this, the non-
183 CG DNA methylation levels in *drm2* at loci that gain H3K27me3 in *drm2*, are equivalent (non
184 significant difference) to the levels of non-CG DNA methylation in WT at loci where DNA
185 methylation is promoted by DRM2 (**Fig.2E**, grey bars). Furthermore, H3K27me3 levels are
186 lower at loci where H3K27me3 is dependent on DRM2 than at loci where H3K27me3 is
187 independent of DRM2 (**Fig. 2F)**. Together, these analyses point to a particular epigenetic state
188 at H3K27me3-marked, DRM2-dependent loci, where both DNA methylation and H3K27me3
189 marks co-localize and accumulate at a lower level than at their other genome-wide targets. This
190 signature appears to underlie a chromatin state _which we coin 'ambivalent'_ whereby the two
191 marks cooperate in their recruitment and which likely contributes to explain the locus-specific
192 and differential DRM2 impacts on H3K27me3 deposition.
193
194 **DNA demethylation impacts H3K27me3 patterning at endogenous TEs.**
195 To further explore the interconnections between DNA methylation and the PcG
196 pathways, we profiled H3K27me3 in the triple DNA demethylase mutant *rdd* (for
197 *ros1/dml1/dml2).* At a subset of loci marked by H3K27me3 in WT and targeted by
198 ROS1/DML1/DML2[37], we observed a loss of H3K27me3 upon DNA hypermethylation (**Fig.**
199 **3A-B and S3A**). This finding indicates that H3K27me3 recruitment at some TEs, which we
200 refer to as "Type 1-targets," could be promoted by active demethylation. This is consistent with

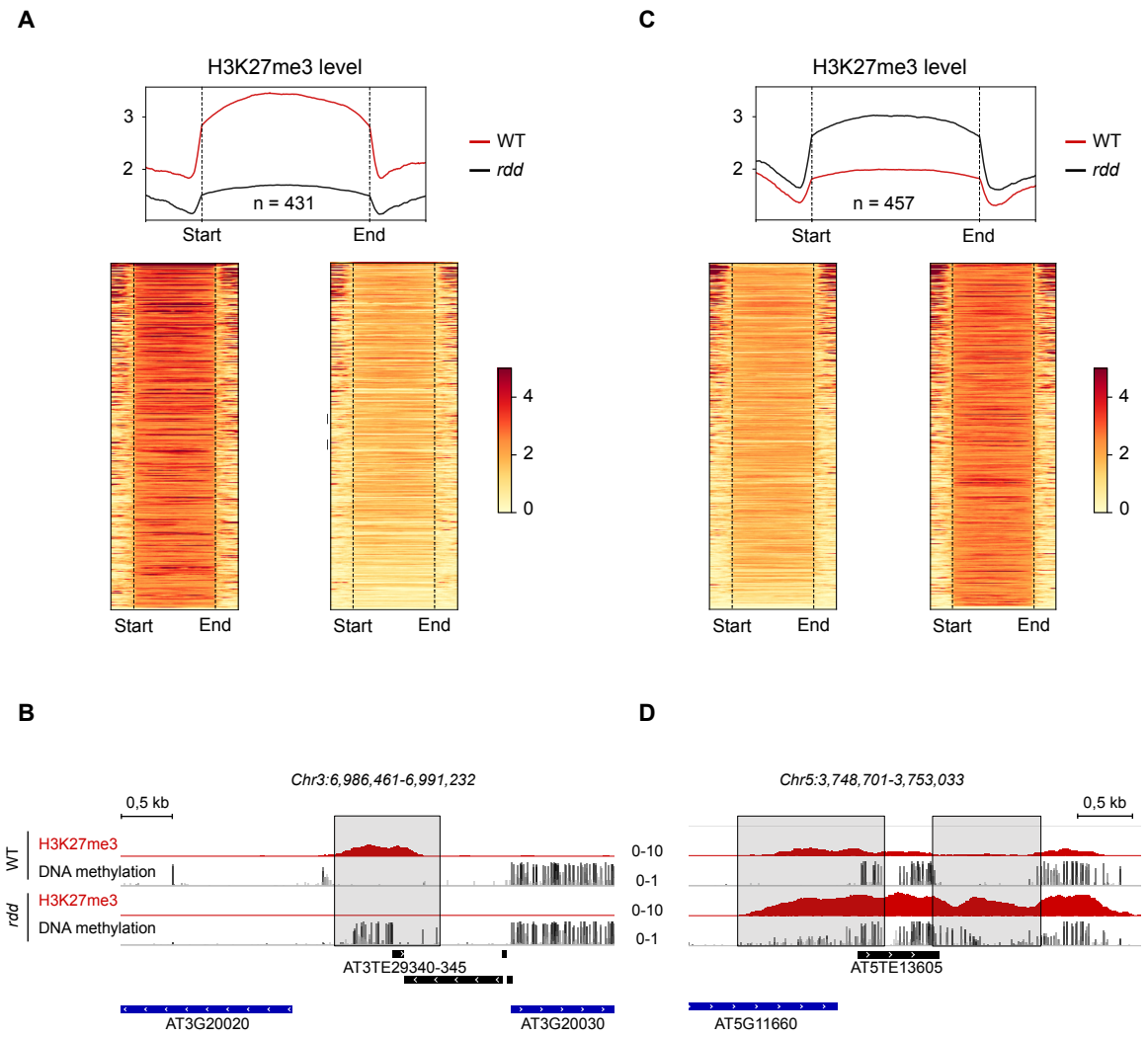

Figure 3. DNA demethylation impacts H3K27me3 patterning at endogenous loci.
(A) Heatmap and metagene showing H3K27me3 levels for loci that loose H3K27me3 peaks in *rdd* compared to WT. **(B)** Representative genome browser view showing H3K27me3 ChIP-seq and DNA methylation BS-seq data in WT and *rdd* mutant. Previously published DMRs are represented by grey boxes) (*Duan et al,. 2015*). **(C)** Heatmap and metagene showing H3K27me3 levels for loci that gain H3K27me3 peaks in *rdd* compared to WT. **(D)** Representative genome browser view showing H3K27me3 ChIP-seq and DNA methylation BS-seq data in WT and *rdd* mutant.

201 the previously described antagonistic effect of DNA methylation on H3K27me3 pathways.
202 Interestingly, and in line with the loss of H3K27me3 observed at some TEs in *drm2* mutants,
203 we also identified a subset of targets where the gain of DNA methylation in *rdd* leads to a gain
204 of H3K27me3 (**Fig. 3C-D** and **S3B**). This subset contains TEs that are not or lowly marked by
205 H3K27me3 in WT, and we refer to them as "Type 2-targets".
206
207 **A targeted DNA methylation approach shows the direct impact of DNA methylation on**
208 **H3K27me3 deposition in a locus-dependent manner**.
209 We next wanted to verify whether the loss of H3K27me3 at the DNA hypermethylated
210 regions was the direct consequence of ectopic DNA methylation. For this purpose, we
211 constructed an inverted repeat transgene to produce small RNAs able to override the dominance
212 of ROS1 activity over RdDM[22] and induce DNA methylation[38] at a specific TE locus
213 (*AT1TE59770*) (**Fig. 4A left panel, Fig. 4B**). In the RNAi lines that we isolated, we observed
214 a gain of DNA methylation in all three sequences contexts (Fig. 4C left panel) and this led to a
215 clear decrease in H3K27me3 at the endogenous TE ("Target 1") compared to the transgenic
216 lines with an unrelated transgene (**Fig. 4D and S4D, left panels**). We thus show for the first
217 time that targeting small RNA-directed DNA methylation to a H3K27me3-marked locus can
218 cause a direct loss of H3K27me3.
219 Likewise, to verify that the gain of H3K27me3 at the DNA hypermethylated regions is
220 the direct consequence of ectopic DNA methylation, we constructed another inverted repeat
221 transgene, this time targeting a locus that gains H3K27me3 in *rdd* (*AT5TE81105*) (**Fig. 4A**
222 **right panel, Fig. 4B**). In the RNAi lines, we observed a gain of DNA methylation in all three
223 sequences contexts (Fig.4C, right panel) and this time an increase in H3K27me3 at the
224 endogenous TE ("Target 2") targeted by RNAi and DNA methylation compared to the
225 transgenic lines containing an unrelated transgene (**Fig. 4D** and **S4D, right panels**). This

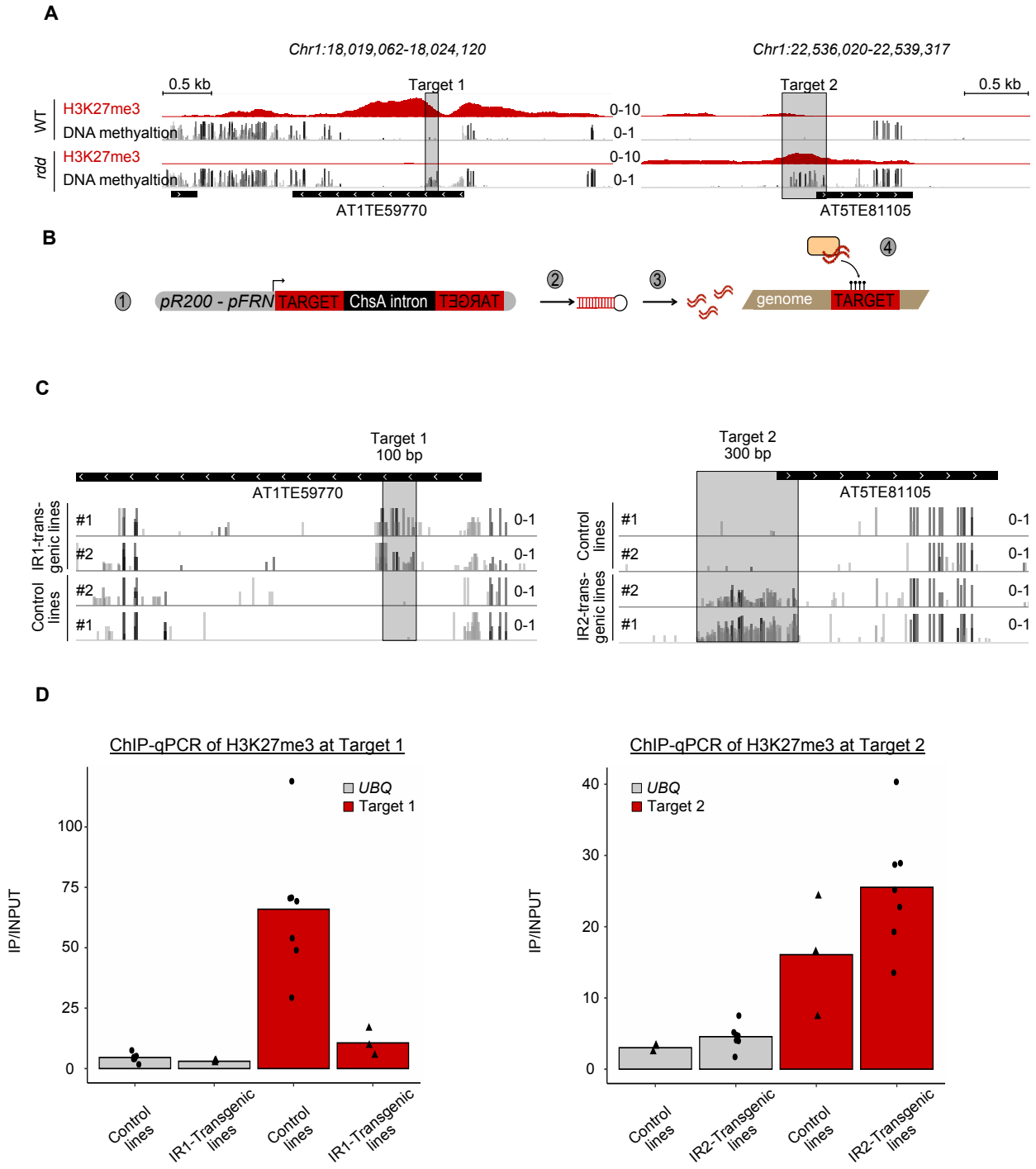

Figure 4. Targeted DNA methylation by inverted-repeats (IR) reveals a dual role of DNA methylation on H3K27me3 patterning at endogenous TEs.
(A) Representative genome browser view showing H3K27me3 and DNA methylation in WT and *rdd* mutant. The region highlighted in grey is a DMR and was cloned as an inverted-repeat (IR) (B) for the experiments shown in C and D. **(B)** Experimental design: **1)** Two TE target regions were chosen (1 and 2); for each target, the sequence was cloned as an inverted repeat (IR) separated by the ChsA intron in the pR200-pFRN vector. **2)** Expression of the IR transgene leads to hairpin formation. **3)** Hairpins are processed by DICER-like proteins into smallRNAs. **4)** Small RNAs induce DNA methylation at the targeted locus. **(C)** Representative genome browser view showing the DNA methylation established at target 1 (**left panel**) and target 2 (**right panel**) in the control (transgenic lines with an unrelated transgene) and IR-transgenic lines. **(D)** ChIP-qPCR analysis of H3K27me3 marks in the control and IR-transgenic lines at Target 1 (IR1) (**left panel**) or Target 2 (IR2) (**right panel**). Data were normalized by the positive control *FLC*; Ubiquitin (*UBQ)* serves as a negative control. Bar plots show the average of H3K27me3 levels from 3 independent lines for IR1 and 7 different lines for IR2; each dot represents the results obtained for one given line. A ChIP replicate of this experiment is shown in Fig.S4.

226 indicates that targeting DNA methylation to a Type 2-TE can increase directly the recruitment
227 of PRC2. This finding is in accordance with the striking observation that H3K27me3 deposition
228 at a newly inserted TE is dependent on DRM2 (**Fig. 1C**) and provides further evidence that
229 DNA methylation can favor H3K27me3 deposition in a locus-specific manner.
230

231 **DISCUSSION**

232 We previously showed that H3K27me3 recruitment and patterning at TEs share
233 commonalities with PcG target genes, such as a partial dependency on PRC1, H2AZ variant
234 incorporation, and the activity of JMJ histone demethylases; besides, sequence recognition
235 motifs such as PREs[39] may also be involved in H3K27me3 deposition since H3K27me3 appears
236 to be instructed by the TE sequence itself[29]. Here, by studying the establishment of H3K27me3
237 on a newly inserted TE sequence, we reveal a novel dependency of PRC2 activity on the DRM2
238 *de novo* methyltransferase, which is TE-specific (**Fig. 5A**). *De novo* deposition of H3K27me3
239 in this context was impaired in the *drm2* mutant, which has never been reported in any organism
240 before.

241 In addition, DRM2 is also required for proper maintenance of H3K27me3 patterns at a
242 subset of loci, as recently reported in rice genes, where H3K27me3 and non-CG methylation
243 can colocalize[40,41]. Accordingly, we show that active DNA demethylation can result in the loss
244 of H3K27me3 at some loci. In contrast, DNA methylation can antagonize H3K27me3, as
245 indicated by the increase of H3K7me3 in *drm2* and the loss of H3K27me3 in *rdd* in different
246 subsets. The antagonistic effect of CG methylation on H3K27me3 deposition was previously
247 shown[31]; however, our results provide two novel insights on that aspect. First, DRM2-mediated
248 CHH methylation can also antagonize PRC2 recruitment, which is consistent with recent
249 H3K27me3 profiles of rice and maize RdDM mutants[42,43]. Second, we demonstrate a novel role
250 for DNA demethylases in promoting PRC2 recruitment. This result is in line with previous

251 observations that ROS1 targets are enriched in H3K27me3[44] and could provide an explanation
252 as to why metazoan TET enzymes are enriched at the hypomethylated DNA promoters of PcG
253 targets[45]. Taken together, our results point to locus-specific rules for H3K27me3 deposition,
254 which would either require DNA methylation or be antagonized by its presence (**Fig. 5B**). Our
255 result suggests a mode of PRC2 recruitment determined by specific epigenetic signatures that
256 include DNA methylation and H3K27me3 levels. PRC2 differential recruitment is also
257 presumably contributed by genetic signatures and the existence of a set of transcription factor
258 (TF) or PRC2 co-factors that may display different affinities for DNA methylation and need to
259 be identified in the future. This does not exclude direct interactions between PRC2 and DRM2
260 or the RdDM machinery in a locus-specific manner or in a context-specific manner (in the
261 context of neo-insertion, for example). In that respect, the transgenic system that we have
262 established provides a framework to dissect the complex interactions between H3K27me3 and
263 DNA methylation during establishment and maintenance throughout generations at a single TE
264 copy in future endeavors.

265 The interconnection that we revealed between *de novo* DNA methylation and deposition
266 of H3K27me3 on newly inserted TEs argues for active cooperation between the two marks at
267 this stage of the TE life cycle. This raises the question as to why such cooperation would take
268 place when a novel copy has just integrated the genome. When they are just inserted into the
269 genome, transposable element sequences are DNA hypomethylated. The targeting of PcG at
270 this stage could thus allow rapid silencing of the element while DNA methylation is being
271 established progressively throughout successive generations. One exciting question to address
272 in the future is whether H3K27me3 persists after one round of reproduction or if DNA
273 methylation quickly becomes dense enough to antagonize H3K27me3 in subsequent
274 generations. If this is the case, H3K27me3 could just be a transient silencing form established
275 quickly by the plant to compensate for low *de novo* DNA methylation in the first generation(s)

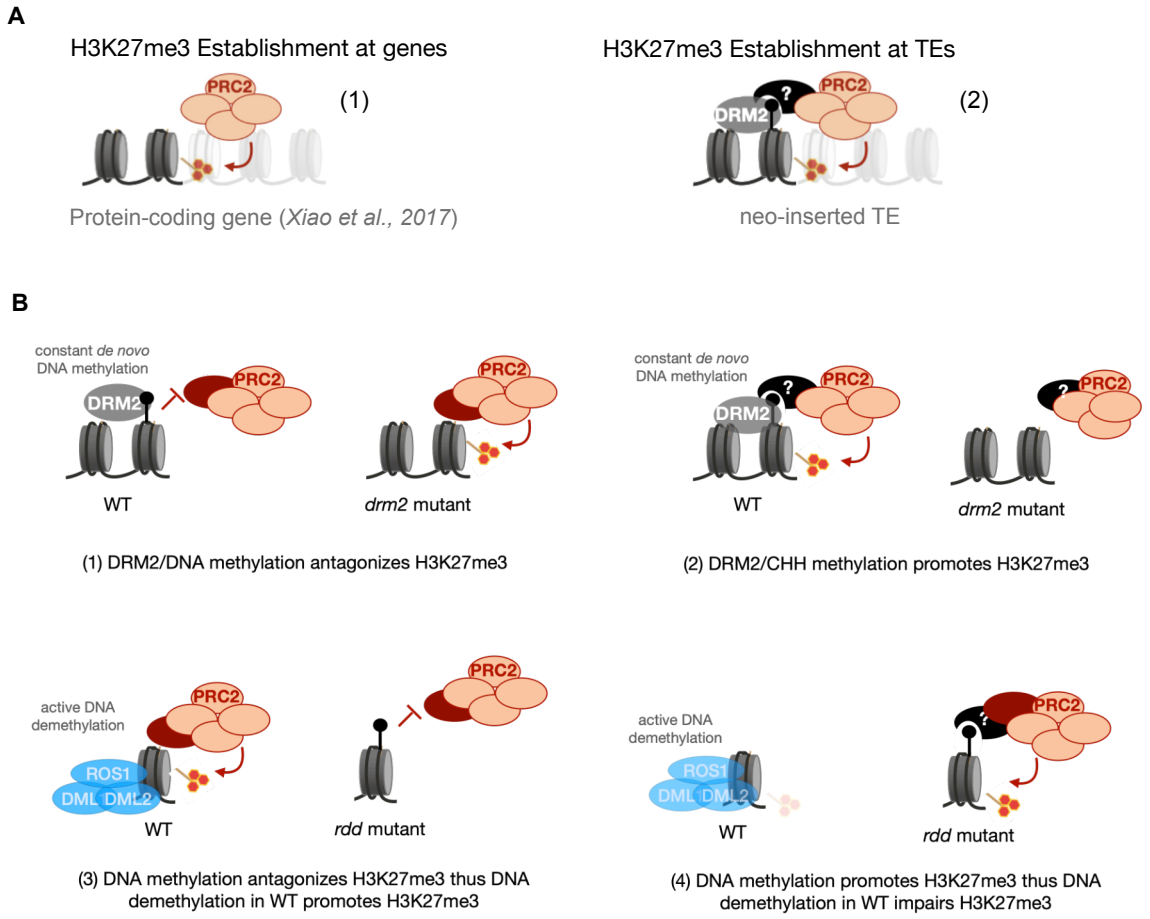

Figure 5. Scenario for differential epigenetic targeting of TEs, in a locus specific manner.
(A) Proposed model for establishment of H3K27me3 at neo-inserted TEs. **1)** PRC2 recruitment on unmethylated protein-coding genes (previously shown to be dependent on specific transcription factors (TF), *Xiao et al., 2017*). **2)** PRC2 recruitment on a neo-inserted TE sequence is DRM2-dependent. Possibly the same TF are involved and may need DNA methylation/DRM2 as a docking site to enhance their recruitment; alternatively, unknown PRC2 accessory proteins with affinity to DNA methylation/DRM2 could be involved. **(B)** Model for locus-specific rules of H3K27me3 maintenance at endogenous TEs. **1)** These TEs are DNA methylated in WT and gain H3K27me3 marks in DNA methylation mutants, notably in *drm2*. DNA methylation presumably prevents the binding of a TF or PRC2 co-factor. Depending on the sequence motif recognized by the TF, the context of DNA methylation preventing TF binding may be different, hence the differences seen in *met1* (our previous work) versus *drm2* (this study) in the gain of H3K27me3. **2**) These TEs are both DNA methylated and marked by H3K27me3 in WT, and they loose both CHH and H3K27me3 in *drm2* mutant. DNA methylation (CHH methylation) would be needed to promote PRC2 recruitment via a TF or PRC2 co-factor which is affine to DNA methylation and requires it as a docking site. Presumably, at these TEs, H3K27me3 is constantly established *de novo*, similarly as DRM2-mediated CHH methylation. **3**) These TEs (Fig.4, "Type1") are marked by H3K27me3 only in WT, and loose H3K27me3 upon gain of DNA methylation in *rdd* mutant. PRC2 recruitment is sensitive to DNA methylation, and active demethylation by DML enzymes promotes H3K27me3 recruitment at these TEs. **4**) These TEs (Fig.4, "Type2") are weakly marked by H3K27me3 and DNA methylation in WT and gain H3K27me3 upon gain of DNA methylation in *rdd*. PRC2 recruitment would be dependent on DNA methylation (as in 2). Together, these TE-specific behaviors point to genetic and epigenetic signatures for PRC2 recruitment and PRC2 antagonism, respectively.

276 after TE neo-insertion. Our study thus points to a synergy between the two silencing pathways,
277 a concept that has also recently emerged at other types of repeats[46,47].

278 For the endogenous TEs, we identified two additional layers of H3K27me3 regulation
279 linked with DNA methylation. First, we demonstrated that DNA demethylases can target
280 specific TEs to promote H3K27me3 deposition instead of DNA methylation. This could be
281 important for TEs, which, as epigenetic modules, negatively impact nearby gene regulation
282 When marked by H3K27me3 instead of DNA methylation, TEs could contribute to a partially
283 repressed state as opposed to a locked silencing state, since H3K27me3 is more plastic and
284 labile in response to developmental or environmental cues. Similarly, the identification of TEs
285 where DNA methylation and H3K27me3 marks not only co-occur but also are interdependent,
286 points to what we refer to as an "ambivalent state", which is actively maintained, and where the
287 loss of one mark is linked to the loss of the other. This could similarly be advantageous for
288 nearby gene regulation; for example, a decrease in CHH methylation in response to certain
289 stresses (such as pathogen-induced stress[48]) could lead to a concomitant decrease in the
290 H3K27me3 mark even if the latter is not sensitive per se to that stress. In that sense, these
291 ambivalent TEs could constitute sensitized modules for the dynamic regulation of nearby genes.
292
293 By connecting PRC2 to DNA methylation at TEs, our work in Arabidopsis provides
294 important insights into the separation and specialization of the two major silencing pathways
295 throughout eukaryotic evolution. We previously proposed that PcG was an ancestral system of
296 TE silencing based on H3K27me3 being the dominant mark at TEs in unicellular organisms or
297 ancestral plants. Furthermore, in ciliates, a small RNA-guided Enhancer of Zeste (Ezl-1, the
298 conserved catalytic subunit of PRC2) results in both H3K27me3 and H3K9 methylation[49,50],
299 which either reflects ciliate-specific catalytic activity or suggests that ancestral PRC2 has both
300 activities. We propose that with the evolution of multicellularity and the need for a dynamic
301 system to control developmental transitions, the PcG and H3K9me2/DNA methylation

302 pathways may have specialized for the silencing of genes and TEs, respectively. Our present
303 results nevertheless show that the major silencing pathways in eukaryotes maintain mechanistic
304 connections despite specialization for different functions in higher plants, which is likely to
305 help their functional cooperation in silencing in specific contexts. Such interconnections may
306 exist in other kingdoms, as suggested by the small RNA-driven deposition of H3K27me3 in *C.*
307 *elegans*[51,52] or the existence of AEBP2, a mammalian PRC2 cofactor that requires DNA
308 methylation for its activity in vitro[53]. Conversely, DNA methylation could be dependent on
309 PRC2, as previously suggested[54,55,] and it would be interesting to investigate this possibility in
310 plants. Future work needs to further decipher the connections between PcG and H3K9/DNA
311 methylation and how they evolved from unicellular to multicellular organisms. This should
312 undoubtedly shed light on the evolution of silencing pathways in eukaryotes and how they
313 shape host genome regulation.
314

315 # MATERIAL AND METHODS

316

317 **Plant material and growth conditions**

318 All the experiments were conducted on *A. thaliana* on ½ MS plates under short light-day
319 conditions (8-h light/16-h dark photoperiod at 22°C). For the transgenic plants shown in Fig. 1,
320 4- week-old rosette leaves were pooled and collected for further ChIP-seq and BS-seq analysis.
321

322 **Mutant lines**

323 We used the *drm1-2 drm2-2* double mutant (Salk-031705, Salk-150863)[5] and the *ros1 dml1*
324 *dml2* triple mutant (Col-0 background, derived from Salk_045303 Salk_056440
325 Salk_131712)[13]
326

327 **Generation of transgenic lines**

328 The *COPIA21* TE sequence was synthesized and cloned and inserted into pUC57 via
329 Genescript. *COPIA21* TE was subsequently cloned and inserted into pCAMBIA3300. The
330 plants were subsequently transformed via *Agrobacterium tumefaciens* floral dip[56]. For the
331 experiments shown in Fig.1, the transgenic plants were selected on Basta after 2 weeks,
332 transferred in soil and 4 weeks old rosettes leaves were collected in pools of 15-20 plants to
333 perform ChIP-seq and BS-seq (on the same ground tissue).

334 RNAi lines were obtained by cloning approximately 250 bp fragments in an inverted orientation
335 via the pFRN vector. The plants were subsequently transformed via *Agrobacterium tumefaciens*
336 floral dip[56,] and T1 plants were selected in-vitro with Kanamycin resistance.

337

338 **Chromatin immunoprecipitation (ChIP) and ChIP–qPCR/sequencing analyses**

339 ChIP experiments were conducted in WT or appropriate mutant lines via an anti-H3K27me3
340 antibody. IP and INPUT DNA were eluted, purified and sequenced (100 bp paired-end;
341 Illumina) by BGI. Reads were mapped via BWA[57] onto TAIR10 *A. thaliana.* Genomic regions
342 significantly marked by H3K27me3 were identified via MACS2[58,] and genes or TEs
343 overlapping these regions were obtained via bedtools[59]. Heatmaps and plotprofiling were
344 generated via bedtools computeMatrix to create a score matrix, and plotHeatmap was used to
345 generate a graphical output of the matrix. For ChIP-seq analyses in *rdd* mutant, regions
346 inherited from Ws-2 *ros1* and *dml2* mutants (Ws background) after backcrossing into Col-0
347 were excluded from analysis as previously described[14].

348

349 **Read count analyses**

350 Reads overlapping with the SNPs (between transgenes and endogenes) at *ATCOPIA21* were
351 extracted, counted and normalized by total read number via SAMtools view. In the control

352 regions (UBQ and FLC), reads were extracted at positions *Chr2:15,143,214* (UBQ) and
353 *Chr5:3,178,750* (1st intron FLC), respectively.
354
355 **Bisulfite-sequencing analyses**
356 DNA was extracted using a standard cetyl trimethylammonium bromide (CTAB)-based
357 protocol. Adapter and low-quality sequences were trimmed via Trimming Galore 0.6.5.
358 Mapping was performed on the TAIR10 genome annotation via Bismark v0.22.2[60] and
359 Bowtie2[61].
360 DNA methylation at *COPIA21* transgenic copies was estimated using the number of transgenic
361 copies (based on read counts in transgenic lines compared to the non-transgenic lines), the total
362 number of *COPIA21* copies (endogene + transgenes), the DNA methylation level of
363 endogenous *COPIA21* in non-transgenic lines and the DNA methylation level of *COPIA21* in
364 transgenic lines. We used the following formula, where *x* stands for the DNA methylation level
365 in a given cytosine context at a single transgenic copy, and then presented on the y axis in %:
366 $$x = \frac{\left(\text{methylation level in transgenic lines} - \frac{\text{methylation levels at endogene in non transgenic lines}}{\text{total number of copies}}\right) \text{x } total\ number\ of\ copies}{\text{number of trangenic copies}}$$
367
368
369 ## ACKNOWLEDGEMENTS
370 We thank N. Bouché for his help with some bioinformatic analyses. We thank ANRJCJC
371 (ANR-19-CE12-0033-01 to A.D.) for funding and the Genome Biology Department of Institut
372 de Biologie Intégrative de la Cellule (I2BC) for support and discussions. We thank the services
373 and platforms of the Institut de Biologie Intégrative de la Cellule (I2BC) for excellent technical
374 support and in particular Véronique Couvreux for excellent plant care. We thank our colleagues
375 of the CNRS Groupements de Recherche "Epiplant" (GDR2027) and "Mobil'ET" (GDR3546)
376 for discussions.

377

378 **REFERENCES**

379 1. Slotkin, R. K. & Martienssen, R. Transposable elements and the epigenetic regulation
380 of the genome. *Nat. Rev. Genet.* **8**, 272–285 (2007).
381 2. Zhang, H., Lang, Z. & Zhu, J.-K. Dynamics and function of DNA methylation in
382 plants. *Nat. Rev. Mol. Cell Biol.* **19**, 489–506 (2018).
383 3. Stroud, H. *et al.* The roles of non-CG methylation in Arabidopsis. *Nat. Struct. Mol.*
384 *Biol.* **21**, 64–72 (2014).
385 4. Lyons, D. B. & Zilberman, D. DDM1 and Lsh remodelers allow methylation of DNA
386 wrapped in nucleosomes. *eLife* **6**, e30674 (2017).
387 5. Cao, X. & Jacobsen, S. E. Role of the Arabidopsis DRM Methyltransferases in De
388 Novo DNA Methylation and Gene Silencing. *Curr. Biol.* **12**, 1138–1144 (2002).
389 6. Chan, S. W.-L. *et al.* RNA Silencing Genes Control de Novo DNA Methylation.
390 *Science* **303**, 1336–1336 (2004).
391 7. Greenberg, M. V. C. *et al.* Interplay between Active Chromatin Marks and RNA-
392 Directed DNA Methylation in Arabidopsis thaliana. *PLOS Genet.* **9**, e1003946 (2013).
393 8. Fultz, D. & Slotkin, R. K. Exogenous Transposable Elements Circumvent Identity-
394 Based Silencing, Permitting the Dissection of Expression-Dependent Silencing. *Plant Cell* **29**,
395 360–376 (2017).
396 9. Ausin, I. *et al.* INVOLVED IN DE NOVO 2-containing complex involved in RNA-
397 directed DNA methylation in Arabidopsis. *Proc. Natl. Acad. Sci. U. S. A.* **109**, 8374–8381
398 (2012).
399 10. Teixeira, F. K. & Colot, V. Repeat elements and the Arabidopsis DNA methylation
400 landscape. *Heredity* **105**, 14–23 (2010).
401 11. Penterman, J. *et al.* DNA demethylation in the Arabidopsis genome. *Proc. Natl. Acad.*
402 *Sci.* **104**, 6752–6757 (2007).
403 12. Ortega-Galisteo, A. P., Morales-Ruiz, T., Ariza, R. R. & Roldán-Arjona, T.
404 Arabidopsis DEMETER-LIKE proteins DML2 and DML3 are required for appropriate
405 distribution of DNA methylation marks. *Plant Mol. Biol.* **67**, 671–681 (2008).
406 13. Zhu, J., Kapoor, A., Sridhar, V. V., Agius, F. & Zhu, J.-K. The DNA
407 glycosylase/lyase ROS1 functions in pruning DNA methylation patterns in Arabidopsis. *Curr.*
408 *Biol. CB* **17**, 54–59 (2007).
409 14. Williams, B. P., Bechen, L. L., Pohlmann, D. A. & Gehring, M. Somatic DNA
410 demethylation generates tissue-specific methylation states and impacts flowering time. *Plant*
411 *Cell* **34**, 1189–1206 (2021).
412 15. Calarco, J. P. *et al.* Reprogramming of DNA methylation in pollen guides epigenetic
413 inheritance via small RNA. *Cell* **151**, 194–205 (2012).
414 16. Ibarra, C. A. *et al.* Active DNA demethylation in plant companion cells reinforces
415 transposon methylation in gametes. *Science* **337**, 1360–1364 (2012).
416 17. Gehring, M. *et al.* DEMETER DNA glycosylase establishes MEDEA polycomb gene
417 self-imprinting by allele-specific demethylation. *Cell* **124**, 495–506 (2006).
418 18. Agius, F., Kapoor, A. & Zhu, J.-K. Role of the Arabidopsis DNA glycosylase/lyase
419 ROS1 in active DNA demethylation. *Proc. Natl. Acad. Sci. U. S. A.* **103**, 11796–11801
420 (2006).
421 19. Morales-Ruiz, T. *et al.* DEMETER and REPRESSOR OF SILENCING 1 encode 5-
422 methylcytosine DNA glycosylases. *Proc. Natl. Acad. Sci. U. S. A.* **103**, 6853–6858 (2006).
423 20. Parrilla-Doblas, J. T., Roldán-Arjona, T., Ariza, R. R. & Córdoba-Cañero, D. Active
424 DNA Demethylation in Plants. *Int. J. Mol. Sci.* **20**, 4683 (2019).

21. Yang, L. *et al.* ROS1-mediated decrease in DNA methylation and increase in expression of defense genes and stress response genes in Arabidopsis thaliana due to abiotic stresses. *BMC Plant Biol.* **22**, 104 (2022).
22. Halter, T. *et al.* The Arabidopsis active demethylase ROS1 cis-regulates defence genes by erasing DNA methylation at promoter-regulatory regions. *eLife* **10**, e62994 (2021).
23. Déléris, A., Berger, F. & Duharcourt, S. Role of Polycomb in the control of transposable elements. *Trends Genet. TIG* **37**, 882–889 (2021).
24. Baile, F., Gómez-Zambrano, Á. & Calonje, M. Roles of Polycomb complexes in regulating gene expression and chromatin structure in plants. *Plant Commun.* **3**, 100267 (2022).
25. Baile, F. & Calonje, M. Dynamics of polycomb group marks in Arabidopsis. *Curr. Opin. Plant Biol.* **80**, 102553 (2024).
26. Wu, H.-W. *et al.* A noncoding RNA transcribed from the () second intron binds to CURLY LEAF and represses expression in leaves. *New Phytol.* **219**, 1480–1491 (2018).
27. Fonouni-Farde, C. *et al.* The Arabidopsis APOLO and human UPAT sequence-unrelated long noncoding RNAs can modulate DNA and histone methylation machineries in plants. *Genome Biol.* **23**, 181 (2022).
28. Hisanaga, T. *et al.* The Polycomb repressive complex 2 deposits H3K27me3 and represses transposable elements in a broad range of eukaryotes. *Curr. Biol. CB* S0960-9822(23)01153–3 (2023) doi:10.1016/j.cub.2023.08.073.
29. Hure, V. *et al.* Alternative silencing states of Transposable Elements in Arabidopsis. 2024.03.16.585326 Preprint at https://doi.org/10.1101/2024.03.16.585326 (2024). *Genome Biology in press* (2025)
30. Mathieu, O., Probst, A. V. & Paszkowski, J. Distinct regulation of histone H3 methylation at lysines 27 and 9 by CpG methylation in Arabidopsis. *EMBO J.* **24**, 2783–2791 (2005).
31. Deleris, A. *et al.* Loss of the DNA Methyltransferase MET1 Induces H3K9 Hypermethylation at PcG Target Genes and Redistribution of H3K27 Trimethylation to Transposons in Arabidopsis thaliana. *PLOS Genet.* **8**, e1003062 (2012).
32. Rougée, M. *et al.* Polycomb mutant partially suppresses DNA hypomethylation–associated phenotypes in Arabidopsis. *Life Sci. Alliance* **4**, (2021).
33. Weinhofer, I., Hehenberger, E., Roszak, P., Hennig, L. & Köhler, C. H3K27me3 Profiling of the Endosperm Implies Exclusion of Polycomb Group Protein Targeting by DNA Methylation. *PLoS Genet.* **6**, e1001152 (2010).
34. Brinkman, A. B. *et al.* Sequential ChIP-bisulfite sequencing enables direct genome-scale investigation of chromatin and DNA methylation cross-talk. *Genome Res.* **22**, 1128–1138 (2012).
35. Statham, A. L. *et al.* Bisulfite sequencing of chromatin immunoprecipitated DNA (BisChIP-seq) directly informs methylation status of histone-modified DNA. *Genome Res.* **22**, 1120–1127 (2012).
36. Zervudacki, J., Agnès, Y., Delase, A., Navarro*, L. & Deleris, A. Transcriptional control and exploitation of an immune-responsive family of plant retrotransposons. *EMBO J.* **37**, e98482 (2018).
37. Duan, C.-G. *et al.* MET18 Connects the Cytosolic Iron-Sulfur Cluster Assembly Pathway to Active DNA Demethylation in Arabidopsis. *PLOS Genet.* **11**, e1005559 (2015).
38. Sigman, M. J. *et al.* An siRNA-guided ARGONAUTE protein directs RNA polymerase V to initiate DNA methylation. *Nat. Plants* **7**, 1461–1474 (2021).
39. Xiao, J. *et al.* Cis and trans determinants of epigenetic silencing by Polycomb repressive complex 2 in Arabidopsis. *Nat. Genet.* **49**, 1546–1552 (2017).

40. Zhou, S. *et al.* Cooperation between the H3K27me3 Chromatin Mark and Non-CG Methylation in Epigenetic Regulation1. *Plant Physiol.* **172**, 1131–1141 (2016).
41. Zhang, W. *et al.* Domains Rearranged Methylase 2 maintains DNA methylation at large DNA hypomethylated shores and long-range chromatin interactions in rice. *Plant Biotechnol. J.* (2023) doi:10.1111/pbi.14134.
42. Hari Sundar G, V. *et al.* Plant polymerase IV sensitizes chromatin through histone modifications to preclude spread of silencing into protein-coding domains. *Genome Res.* **33**, 715–728 (2023).
43. Guo, W., Wang, D. & Lisch, D. RNA-directed DNA methylation prevents rapid and heritable reversal of transposon silencing under heat stress in Zea mays. *PLoS Genet.* **17**, e1009326 (2021).
44. Tang, K., Lang, Z., Zhang, H. & Zhu, J.-K. The DNA demethylase ROS1 targets genomic regions with distinct chromatin modifications. *Nat. Plants* **2**, 16169 (2016).
45. Verma, N. *et al.* TET proteins safeguard bivalent promoters from de novo methylation in human embryonic stem cells. *Nat. Genet.* **50**, 83–95 (2018).
46. Eimer, H. *et al.* RNA-Dependent Epigenetic Silencing Directs Transcriptional Downregulation Caused by Intronic Repeat Expansions. *Cell* **174**, 1095-1105.e11 (2018).
47. Sureshkumar, S. *et al.* SUMO protease FUG1, histone reader AL3 and chromodomain protein LHP1 are integral to repeat expansion-induced gene silencing in Arabidopsis thaliana. *Nat. Plants* **10**, 749–759 (2024).
48. Deleris, A., Halter, T. & Navarro, L. DNA Methylation and Demethylation in Plant Immunity. *Annu. Rev. Phytopathol.* **54**, 579–603 (2016).
49. Miró-Pina, C. *et al.* Paramecium Polycomb repressive complex 2 physically interacts with the small RNA-binding PIWI protein to repress transposable elements. *Dev. Cell* **57**, 1037-1052.e8 (2022).
50. Balan, T., Lerner, L. K., Holoch, D. & Duharcourt, S. Small-RNA-guided histone modifications and somatic genome elimination in ciliates. *WIREs RNA* **15**, e1848 (2024).
51. Mao, H. *et al.* The Nrde Pathway Mediates Small-RNA-Directed Histone H3 Lysine 27 Trimethylation in *Caenorhabditis elegans*. *Curr. Biol.* **25**, 2398–2403 (2015).
52. Seroussi, U. *et al.* Mechanisms of epigenetic regulation by *C. elegans* nuclear RNA interference pathways. *Semin. Cell Dev. Biol.* **127**, 142–154 (2022).
53. Wang, X. *et al.* Molecular analysis of PRC2 recruitment to DNA in chromatin and its inhibition by RNA. *Nat. Struct. Mol. Biol.* **24**, 1028–1038 (2017).
54. Schlesinger, Y. *et al.* Polycomb-mediated methylation on Lys27 of histone H3 pre-marks genes for de novo methylation in cancer. *Nat. Genet.* **39**, 232–236 (2007).
55. Viré, E. *et al.* The Polycomb group protein EZH2 directly controls DNA methylation. *Nature* **439**, 871–874 (2006).
56. Clough, S. J. & Bent, A. F. Floral dip: a simplified method for Agrobacterium-mediated transformation of Arabidopsis thaliana. *Plant J. Cell Mol. Biol.* **16**, 735–743 (1998).
57. Li, H. & Durbin, R. Fast and accurate short read alignment with Burrows-Wheeler transform. *Bioinforma. Oxf. Engl.* **25**, 1754–1760 (2009).
58. Zhang, Y. *et al.* Model-based analysis of ChIP-Seq (MACS). *Genome Biol.* **9**, R137 (2008).
59. Quinlan, A. R. & Hall, I. M. BEDTools: a flexible suite of utilities for comparing genomic features. *Bioinforma. Oxf. Engl.* **26**, 841–842 (2010).
60. Krueger, F. & Andrews, S. R. Bismark: a flexible aligner and methylation caller for Bisulfite-Seq applications. *Bioinforma. Oxf. Engl.* **27**, 1571–1572 (2011).
61. Langmead, B., Trapnell, C., Pop, M. & Salzberg, S. L. Ultrafast and memory-efficient alignment of short DNA sequences to the human genome. *Genome Biol.* **10**, R25 (2009).

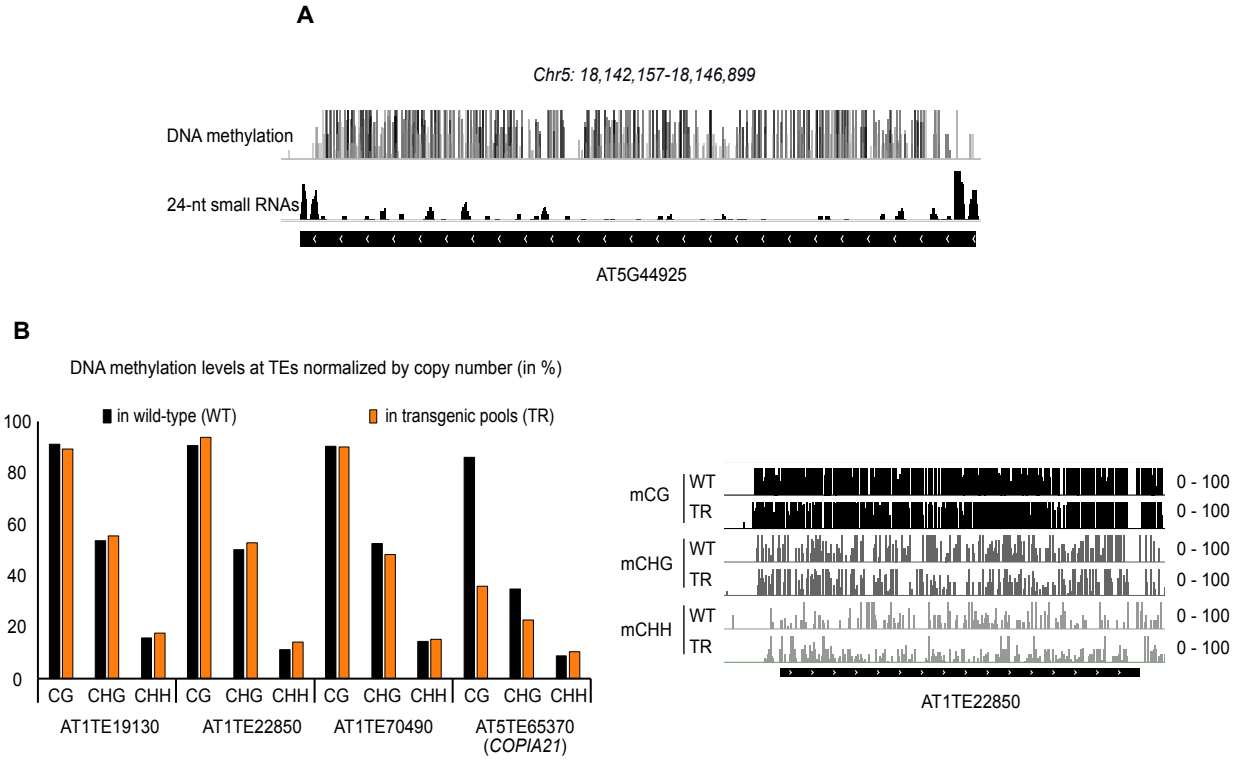

Figure S1. Role of DRM2 in the establishment of *de novo* H3K27me3 at a neo-inserted TE transgenic sequence. (A) Representative genome browser view of DNA methylation (overlay of mCG in black, mCHG in dark grey and mCHH in light grey) and 24-nt small RNAs levels at *COPIA21* in wild-type (WT). **(B) Left panel**: Barplot showing the DNA methylation levels in each cytosine context at different endogenous TEs in WT (black bars) and in transgenic pools (orange bars). **Right panel**: Representative genome browser view of DNA methylation status (CG: black, CHG: dark grey, CHH : light grey) at *AT1TE22850* in wild-type (WT) and in transgenic pools (TR).

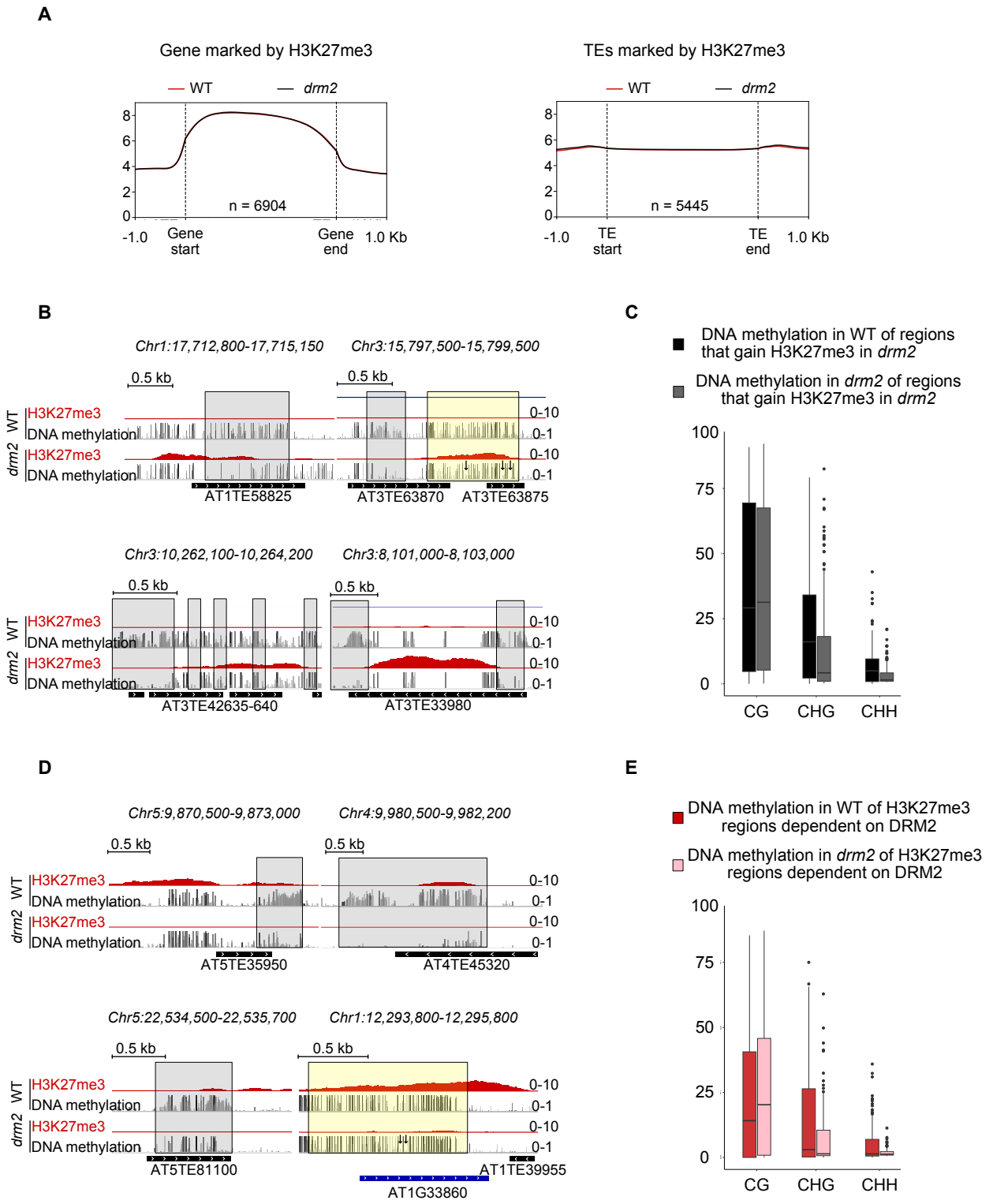

Figure S2. Role of DRM2 in the recruitment of H3K27me3 at endogenous loci.
(A) Metagenes showing H3K27me3 level for genes (**left panel**) and TEs (**right panel**) marked by H3K27me3, in WT and *drm2* mutant. **(B)** Representative genome browser views showing H3K27me3 ChIP-seq and DNA methylation BS-seq data in WT and *drm2* mutant. Gain of H3K27me3 in *drm2* compared to WT is either associated with previously published DMRs (grey boxes) (*Stroud et al, 2013*) or DNA methylated regions that loose several methylated cytosines (yellow box; the arrows indicate the loss of several mCHH). **(C)** Boxplot showing DNA methylation in three contexts for different H3K27me3 peak regions (i.e. peak+500bp on the sides to account for any effect of DNA methylation patches on peak edges. Black and grey bars show the DNA methylation levels in the same regions, either in WT or in *drm2*, respectively. These regions correspond to peaks of H3K27me3 gained in *drm2* mutant. **(D)** Representative genome browser views showing H3K27me3 ChIP-seq and DNA methylation BS-seq data in WT and *drm2* mutant. Loss of H3K27me3 in *drm2* compared to WT is either associated with previously published DMRs (grey boxes) (*Stroud et al, 2013*) or DNA methylated regions that loose several methylated cytosines(yellow box; the arrows indicate the loss of several mCHH). **(E)** Boxplot showing DNA methylation in three contexts for different H3K27me3 peak regions (i.e. peak+500bp on the sides to account for any effect of DNA methylation patches on peak edges). Red and pink bars show the DNA methylation levels in the same regions, either in WT or in *drm2*, respectively. These regions correspond to peaks of H3K27me3 dependent on DRM2 in WT.

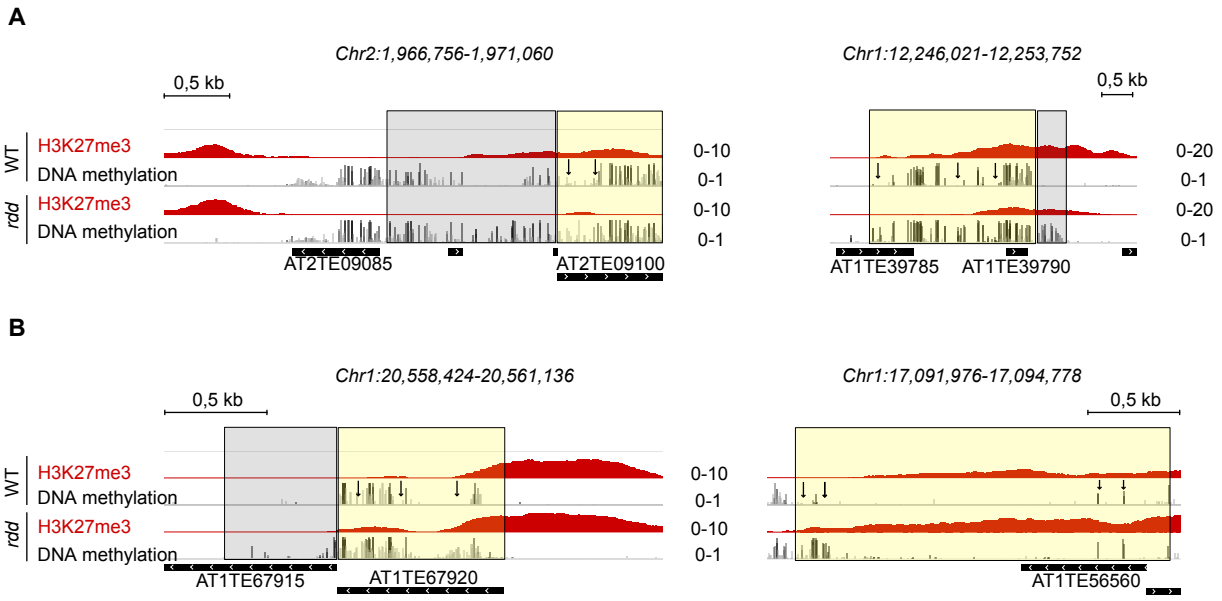

Figure S3. DNA demethylation impacts H3K27me3 patterning at endogenous loci.
Representative genome browser views showing H3K27me3 and DNA methylation in WT and *rdd* mutant. Regions highlighted in grey are DMRs previously identified (*Duan et al,. 2015*) whereas regions highlighted in yellow are regions that were not previously identified as DRMs despite some changes in cytosine methylation (black arrows). **(A)** and **(B)** panels show loss and gain of H3K27me3 in *rdd,* respectively.

A

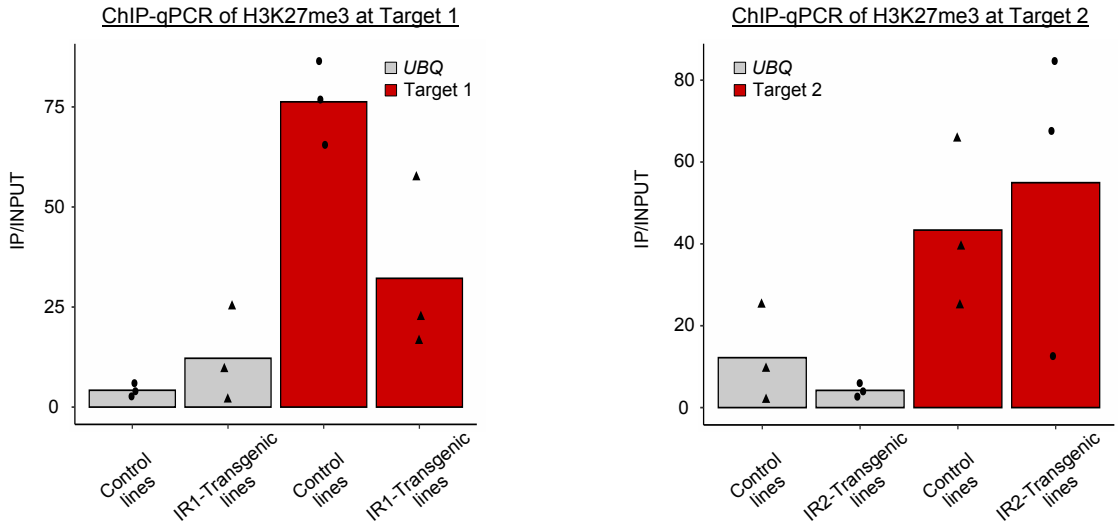

Figure S4. Targeted DNA methylation by inverted-repeats (IR) reveals a dual role of DNA methylation on H3K27me3 patterning at endogenous TEs.
(A) ChIP-qPCR analysis of H3K27me3 marks in the control and IR-transgenic lines at Target 1 (IR1) (**left panel**) or Target 2 (IR2) (**right panel**). Here, a biological replicate of the experiment in Fig.4 (ChIP replicate on 3 lines) is presented . Data were normalized by the ChIP positive control *FLC*; Ubiquitin (*UBQ*) serves as a negative control. Bar plots show the average of H3K27me3 levels from three different control and transgenic lines where each dot represents one given transgenic line. Biological replicates are shown separately in Fig.4 and Fig.S4 because of the difference in ChIP efficiencies between the two batches of ChIP experiments.